

TOWARDS MORE REALISTIC MODELS OF GENOMES IN POPULATIONS: THE MARKOV-MODULATED SEQUENTIALLY MARKOV COALESCENT

JULIEN Y. DUTHEIL

The development of coalescent theory paved the way to statistical inference from population genetic data. In the genomic era, however, coalescent models are limited due to the complexity of the underlying ancestral recombination graph. The sequentially Markov coalescent (SMC) is a heuristic that enables the modelling of complete genomes under the coalescent framework. While it empowers the inference of detailed demographic history of a population from as few as one diploid genome, current implementations of the SMC make unrealistic assumptions about the homogeneity of the coalescent process along the genome, ignoring the intrinsic spatial variability of parameters such as the recombination rate. Here, I review the historical developments of SMC models and discuss the evidence for parameter heterogeneity. I then survey approaches to handle this heterogeneity, focusing on a recently developed extension of the SMC.

1. MODELLING THE EVOLUTION OF GENOMES IN POPULATIONS

When modelling the evolution of large genomic sequences at the population level, in particular for sexually reproducing species, a key biological mechanism to account for is meiotic recombination, which shuffles genetic material at each generation. We first introduce the concept of the ancestral recombination graph, needed to represent the complete genealogy of a sample undergoing recombination. We then review the statistical approaches used to fit models accounting for recombination to population genomics data.

1.1. The ancestral recombination graph. The evolution of the set of sequences carried by all individuals forming a population, generation after generation, can be modelled by a stochastic process, where each individual leaves a variable number of descendants in the next generation. As a result, at any position of the sequence, the *genealogy* of a sample of n individuals can be described by a tree (Figure 1A) [35]. The tips of the tree represent the sampled individuals and the inner nodes their common ancestors. In the case of sexually reproducing organisms, which will be the focus of this chapter, the genealogy is not identical for every position in the sequence. During *sexual reproduction*, two individuals contribute part of their sequence to their descendant(s) in the next generation. The mechanism of *recombination* is responsible for randomly sampling the new sequence from the two parental ones (Figure 1B). How often and where the recombination points occur will be discussed in Section 2. The consequences of the recombination process can be stated as: (1) the genealogy of the sequence on

the left of a recombination breakpoint potentially differs from the genealogy of the sequence on the right, (2) the genealogy at two positions in the sequence are more likely to differ as the distance between the two points is large, and (3) the genealogy of the complete sequence can no longer be described by a single tree, but by a collection of such trees and associated breakpoints. This tree and breakpoints collection can be represented as a single graph, called the *ancestral recombination graph (ARG)* (Figure 1C) [25]. The complexity of the ARG grows with the number of individuals (which dictates the size of the underlying trees) and the number of recombination events (which determines how many trees are needed to represent the history of the full sequences). The ARG represents the complete history of the sampled individuals, where the trees at each position (referred to as the “marginal genealogies”) are embedded [49]. It describes the history of each segment of the sampled sequences, tracing back their ancestors in potentially distinct individuals. Such segments, which have left descendants in the sample, are termed *ancestral*. Contained in the ARG is also the history of some *non-ancestral segments*, which did not leave a descendant in the sample, but were once part of a sequence that contained both ancestral and non-ancestral segments (Figure 1D).

The characteristics of the ARG are determined by the demography of the population (the history of population size changes), the recombination landscape (where do the recombination events occur), but also the selective forces acting on the sequence, as natural selection influences the distribution of the number of descendants for each individual, based on the nature of the sequences themselves. While the ARG contains the signature of the biological processes that shaped the genome sequences, it is unfortunately not directly accessible. In order to access the embedded information, it is necessary to model the evolution of sequences in populations.

1.2. The coalescent with recombination as a chronological process.

When modelling evolution, the most intuitive approach is to consider the process chronologically, that is, to model the state of the system generation after generation. One of the most simple models, the so-called *Wright–Fisher process*, considers that the gametes forming one generation are a random sample of the gametes produced at the previous generation, that is, reproduction is a purely random process where each individual has the same a priori chance to contribute to the next generation. In addition, the population has a finite, constant size. A similar model, termed the *Moran process*, considers a slightly different set-up with overlapping generations [50]. The Wright–Fisher and Moran processes can both accommodate recombination, modelled by randomly choosing a breakpoint along the genome and exchanging the parental genetic segments (see the contribution of Baake and Baake [6] in this volume). In such processes, the fate of a genetic variant is purely stochastic and governed only by the population size.

When conditioning on a sample of the result of the evolutionary process, a backwards-in-time modelling is used. Each sequence in the sample represents a lineage, and the aim of the model is to determine which lineages find a common ancestor in the past and when. Every time two lineages *coalesce* into a common ancestor, the number of lineages to model is reduced by one,

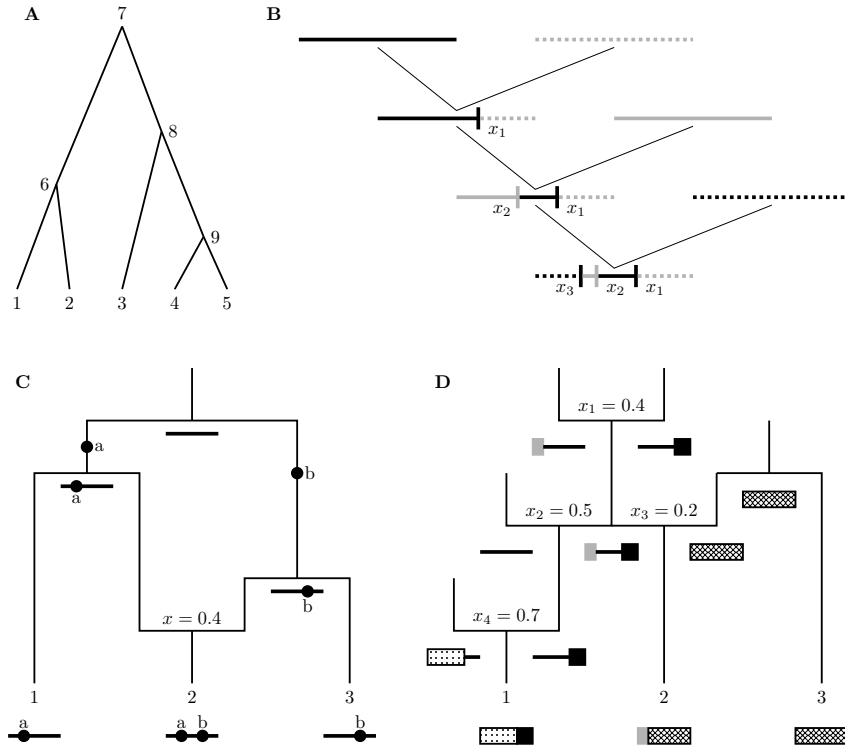


FIGURE 1. Genealogies and recombination: relationships between individuals and along sequences. A) example genealogy of a sample of five individuals at a given position in the sequences, under a Kingman coalescent. Tip nodes represent the samples (1-5) and inner nodes their common ancestors (6-9). B) illustration of the recombination tree resulting from a process without coalescence (large number approximation): two chromosomes (solid black and dotted grey) are paired during sexual reproduction and exchange segments at a breakpoint x_1 . At the next generation, the descendant sequence recombines with another sequence (solid grey) at another breakpoint x_2 , etc. The sequence of any sampled individual is therefore a mosaic of segments with distinct ancestors separated by a series of breakpoints (x_1, x_2, x_3). C) a simple ancestral recombination graph (ARG) representing the genealogy of a sample of size three with one recombination event. The ARG is a combination of a coalescence tree (as in A) and a recombination tree (as in B). For ease of interpretation, two mutation events, $\bullet a$ and $\bullet b$ have been added. The relative coordinate of the recombination event is also indicated: $x = 0.4$, assuming a total sequence length of 1. D) partial graph showing the different classes of recombination events. Ancestral segments are depicted as filled rectangles, while non-ancestral segments are shown as simple lines (subfigure created after Figure 1 in [47]).

until the last common ancestor of the sample is reached. This process of lineages merging backwards in time is termed the *coalescent* [35].

The probability that two lineages merge at a given generation back in time depends on the population size. When the population size is constant in time, the number of generations until coalescence follows a geometric distribution with parameter $\frac{1}{2 \cdot N_e}$, where N_e is the *effective population size*. Assuming a large N_e , this discrete-time coalescent is well approximated by a continuous-time coalescent, where the divergence time between two sequences follows an exponential distribution with average $2 \cdot N_e$ generations. For convenience, time is, therefore, measured in ‘‘coalescence’’ units equal to $2 \cdot N_e$, so that the mean divergence time between two sequences in a sample is equal to 1.

In the *coalescent with recombination* process, recombination events are modelled in addition to coalescence events [30]. Backwards-in-time, a lineage undergoing a recombination event splits in two, the left and right sequences having distinct ancestors. Since the rates of coalescence and recombination events, at any time point, depend only on the current lineages, the process is Markovian in time [63]. This property enabled the development of simulation procedures and inference methods, allowing the estimation of various parameters by integrating over the unknown genealogy of a sample (e.g. [2, 14]). Such methods, however, do not scale well with the length of the modelled sequences, as the number of events in the underlying ARG grows with the sequence length [20], preventing efficient integration even with Markov chains Monte-Carlo [75]. These methods are, therefore, restricted to small samples with relatively few loci.

1.3. The coalescent with recombination as a sequential process.

Following the initial work by Simonsen and Churchill [63], Wiuf and Hein extended the two-loci model of coalescence with recombination to multiple loci [82]. The resulting process models the ARG sequentially along the genome rather than chronologically. The resulting *sequential coalescent with recombination* aims at modelling the genealogy of the sample at position i given the genealogies at previous positions. In fact, genealogies at two distinct positions in the sequence are not independent: they are identical if no recombination event occurred between the two positions since the last common ancestor of the sample and can only differ if at least one recombination event occurred. Despite this intuitive correlation structure, the coalescent with recombination is not Markovian along the sequence. Computing the probability distribution of the marginal genealogy at a given position proved to be quite challenging because of long-range dependencies, the genealogy at position i depending not only on the genealogy at position $i - 1$, but on the genealogy at all positions 1 to $i - 1$.

With the goal to simplify the likelihood calculation under the coalescent with recombination, McVean and Cardin proposed an approximation where certain types of coalescence events are ignored [49]. An intuitive description of the simplified process was provided by Marjoram and Wall [47], who recognised five types of recombination events on the ARG, based on the type of segments in the parental sequences on both sides of the recombination event (Figure 1D): type 1 events occur in ancestral segments (events at

x_3 and x_4 in Figure 1D) while types 2-5 occur in non-ancestral segments. Type 2 events occur in so-called *trapped genetic material* [57], that is, non-ancestral segments flanked on both sides by ancestral segments (event at x_1 in Figure 1D). Events of types 3, 4, and 5 occur in non-ancestral segments only flanked by non-ancestral segments on one or both sides (e.g. event at x_2 in Figure 1D). Such events (3, 4 and 5) do not affect the sample generated by the corresponding ARG, and therefore do not impact the likelihood of the sample given the ARG. They can therefore be ignored without introducing any additional hypotheses, see [82] (types 4 and 5) and [31] (types 3, 4 and 5). The process of McVean and Cardin, which was further improved by Marjoram and Wall [47] and Hobolth and Jensen [29] also ignores type 2 recombination events, that is, recombination events occurring in trapped genetic material [57]. Doing so implies ignoring potential long-range dependencies between loci, and the distribution of samples generated by this approximated process is, therefore, different from that of the standard coalescent with recombination. The approximated process, however, has the additional property that the distribution of genealogies at position i is only dependent on the genealogy at position $i - 1$, and is, therefore, Markovian along the sequence. Such a process is referred to as the *sequentially Markov coalescent (SMC)* [49, 47]. Importantly, the SMC process generates samples with patterns of genetic diversity that are very similar to the ones generated by the full coalescent process [49]. The SMC, in particular, can be seen as a first-order Markov approximation of the true coalescent with recombination process [81], and higher order extensions have been introduced [66]. Furthermore, the Markov property enables very efficient likelihood calculation using dynamic programming algorithms to integrate over all ARGs. Such methodology comes from the field of *hidden Markov models (HMM)*, which we introduce in the next section.

1.4. Coalescent hidden Markov models. Because of the SMC approximation, likelihood calculation under a coalescent with recombination process represents a classical bioinformatic problem where the probability of an observed state in the sequence depends on an unobserved state, which is then said to be hidden. In the case studied here, the observed states are sequence polymorphisms (between 2 or more individual sequences) and the hidden states are the underlying marginal genealogies. HMMs have been broadly used in sequence analysis [15]. *Coalescent hidden Markov models (CoalHMM)* refer to HMMs where the hidden states are genealogies. It was introduced by Hobolth et al [27] as a name of the first model developed, which we introduce later in this section, but was then extended to generally encompass a full class of models [65] (Figure 2).

We note as $\{\mathcal{A}_i\}_{1 \leq i \leq L}$ the site-specific random variable of observed states in a sample of M sequences of length L . Such states (noted $\{A_g\}_{1 \leq g \leq S}$) are, in the general case, a combination of the four nucleotides A , C , G and T (one per modelled sequence), with the possibility to additionally account for missing data (coded as N), so that $\{A_g\}_{1 \leq g \leq S} \in \{A, C, G, T, N\}^M$ and $S < 5^M$ because of symmetry relationships between trees making some of them unidentifiable. We note as $\{x_i\}_{1 \leq i \leq L}$ a particular realisation of

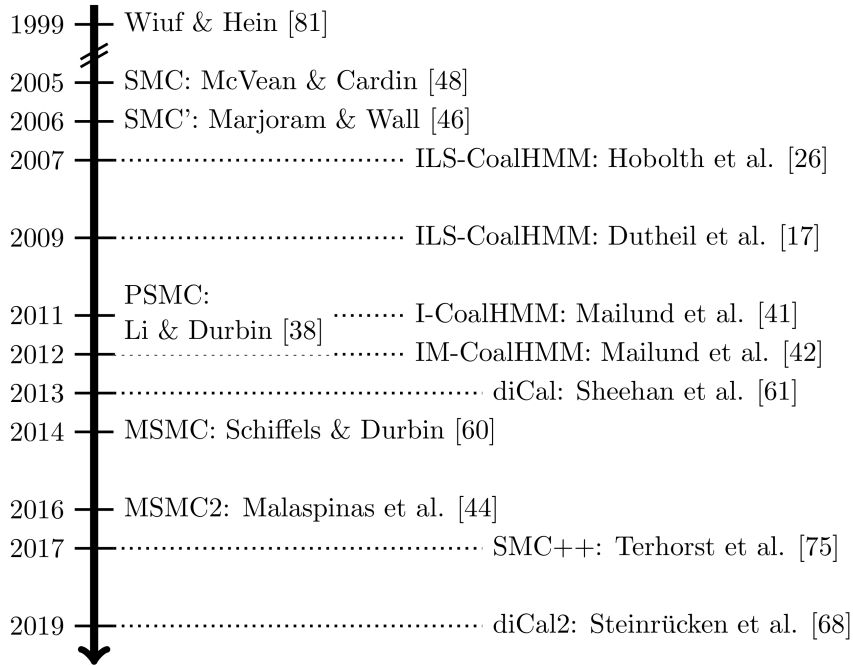


FIGURE 2. Chronology of sequentially Markov coalescent (SMC) and coalescent hidden Markov models (CoalHMM). PSMC: pairwise SMC. MSMC: multiple SMC. ILS: incomplete lineage sorting. I: isolation model. IM: isolation with migration model.

$\{\mathcal{A}_i\}_{1 \leq i \leq L}$, that is, the sequence data. Furthermore, we note as $\{\mathcal{H}_i\}_{1 \leq i \leq L}$ the site-specific random variable describing the marginal genealogies at each position in the sequences. In the general case, such genealogies are rooted trees with M leaves.

In HMM terminology, the probabilities of observing the sequence data x_i at a given position i given a realisation of \mathcal{H}_i , $\Pr(\mathcal{A}_i = x_i | \mathcal{H}_i)$, are called the *emission probabilities*. \mathcal{H}_i is a random variable that has a continuous distribution. To make likelihood calculations tractable, this distribution is discretized, so that \mathcal{H}_i can take a finite number n of hidden states, $\{H_j\}_{1 \leq j \leq n}$. Under a discretised distribution of hidden states, the emission probabilities for each position i , hidden state k can be more explicitly written as:

$$(1) \quad e_{i,k}(x) = \Pr(\mathcal{A}_i = x | \mathcal{H}_i = H_k).$$

We further introduce the so-called *transition probability* of a genealogy H_j at position $i - 1$ to a genealogy H_k at position i as

$$(2) \quad q_{i,j,k} = \Pr(\mathcal{H}_i = H_k | \mathcal{H}_{i-1} = H_j).$$

Given the set of emission and transition probabilities we can then write the likelihood of the data by recursion. We define $F_{i,k}$ the joint probability of the data (observed states) x_1, \dots, x_i at positions 1 to i and the ancestral

genealogy H_k at position i as:

$$(3) \quad F_{i,k} = \Pr(x_1, \dots, x_i, H_k) = \begin{cases} f_k & \text{if } i = 0 \\ e_{i,k}(x_i) \cdot \sum_j q_{i,j,k} \cdot F_{i-1,j} & \text{if } i > 0 \end{cases},$$

where $\{f_k\}_{1 \leq k \leq n}$ denotes some initial conditions. These conditions may be set to $1/n$, or to the stationary distribution of the Markov chain (providing it exists). Equation (3) is called the *forward algorithm* and allows for the computation of the likelihood of the sequences as

$$(4) \quad \mathcal{L} = \sum_k F_{L,k}.$$

This recursion is an example of dynamic programming, allowing for the integration over all possible ARGs very efficiently, as it scales in $\mathcal{O}(L \cdot n^2)$. The symmetry relationships in the transition matrix and the relatively low frequency of the observed heterozygous states, however, allow for further improvement of the run time of the forward algorithm [26, 76, 59].

The likelihood function depends on a set of parameters Θ , which includes the demographic model (effective population size and its variation) and the recombination rate. More complex models can be implemented, for instance allowing for population structure. These parameters can affect either the emission probabilities $e_{i,k}(x)$, the transition probabilities $q_{i,j,k}$, or both. The emission and transition probabilities define the type of model used. Importantly, most models assume that the process is homogeneous along the sequence, so that both $e_{i,k}(x)$ and $q_{i,j,k}$ are actually independent of i . In the following, we will review several examples of coalescent HMM models.

1.5. The two-genome case. When the genome sample consists only of two genomes, the marginal genealogies have a more simple encoding consisting of a single (continuous) number representing the time to the most recent common ancestor (TMRCA) of the two sequences. The TMRCA can be further discretised into n hidden states, each represented by a mean value $(t_j)_{1 \leq j \leq n}$. The transition probabilities between the hidden states can be calculated under the SMC. Variants of this model were developed independently by Li and Durbin [39] and Mailund et al [42]. In the latter, the two genomes come from two distinct populations that diverged at a time τ units ago (Figure 3A). The common ancestral population is assumed to have a constant effective population size θ_{anc} . The TMRCA $(t_j)_{1 \leq j \leq n}$ follows an exponential distribution shifted by an amount of τ . Mailund and collaborators applied this model to the newly sequenced genomes of two Orangutan subspecies in order to estimate their ancestral effective population size and the time of their last genetic exchange. They further extended this model to allow for a period of gene flow after the initial separation of the two populations [43].

In the Li and Durbin model, named pairwise sequentially Markov coalescent (PSMC), the two genomes come from a single population. This approach was further improved by Schiffels and Durbin [61], who used a more accurate recombination model. The authors consider a demographic model where the effective population size is piecewise constant over a given number of epochs (Figure 3A). The parameters of the model consist of the

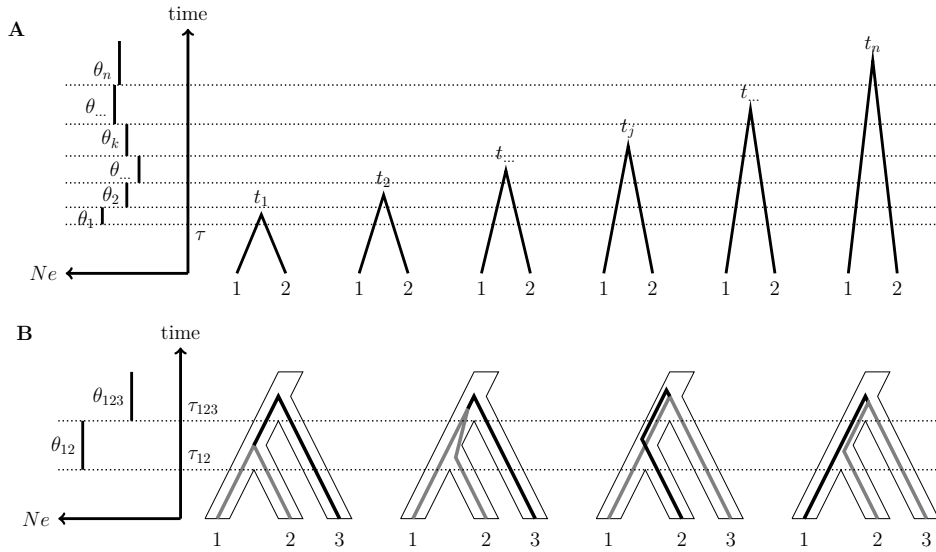


FIGURE 3. Demographic models and hidden states for CoalHMM with two and three sequences. A: Pairwise SMC. Hidden states correspond to discretised divergence times between two sequences. Parameters of the model potentially contain a species divergence time τ and several epochs of constant effective population sizes θ_k . The CoalHMM model of Mailund et al. [42] uses only one epoch and θ , the corresponding states t_j being, therefore, drawn from the exponential distribution with mean $2 \cdot \theta$, shifted by τ . The PSMC model of Li and Durbin [39], assumes a skyline model of multiple epochs, yet with individuals from the same population ($\tau = 0$). B: CoalHMM with three sequences and ILS. The hidden states correspond to four genealogies that differ both in time and order of the coalescence events. The model assumes constant but distinct ancestral effective population sizes θ_{12} and θ_{123} , as well as the two species divergence times τ_{12} and τ_{123} .

set of ancestral sizes, as well as the recombination rate, presumed to be constant along the sequences. While the epochs of the demographic model and the discretisation scheme used for the divergence time are distinct aspects, it is convenient to have some overlap between the two, providing that there are at least as many hidden states as epochs (otherwise some parameters would become unidentifiable). Li and Durbin proposed to consider one hidden state per epoch, so that each segment is represented by one value of t_j and one value of θ_j (Figure 3A). By estimating one θ per epoch, the PSMC model allows the reconstruction of a “skyline” plot where population size varies in time, from present to the distant past (Figure 4). This method was applied to data from the 1000 Genomes Project [1] in order to infer the demographic history of distinct populations, which show the signature of the out-of-Africa bottleneck.

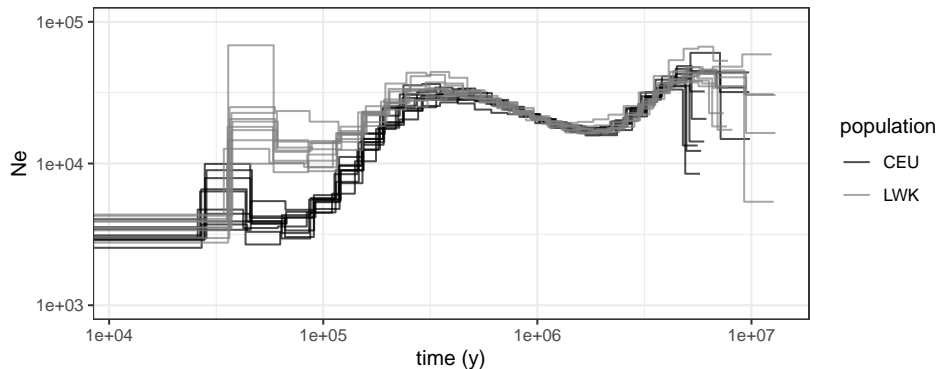


FIGURE 4. Demographic inference under the PSMC. The MSMC2 software was used independently on 20 diploid individuals from the 1000 genomes project [1], 10 from the CEU population (Utah residents with European ancestry) and 10 from the LWK population (Luhya in Webuye, Kenya). MSMC2 was run on data from chromosome 9 only, with default parameters. The results show that individuals with European ancestry underwent a stronger bottleneck between 50 and 100 ky ago, corresponding to the out-of-Africa event.

The two approaches of Li and Durbin and Mailund et al. further differ in their calculation of the emission probabilities. Focusing on the population level and a relatively short time span of ~ 1 Myr, Li and Durbin consider an *infinite sites model* where only one mutation per site can happen. They further consider all types of mutations as equally probable and ignore the biochemical nature of the underlying nucleotides. This reduces the number of observed states to three types: homozygous (the two sequences are identical at a given position), heterozygous (the two sequences differ at a given position), and unknown (at least one sequence has an unresolved state at that position). The emission probabilities then take the simple form:

$$(5) \quad e_{i,j,\text{homozygous}} = \exp(-\theta \cdot t_j)$$

$$(6) \quad e_{i,j,\text{heterozygous}} = 1 - \exp(-\theta \cdot t_j)$$

$$(7) \quad e_{i,j,\text{unknown}} = 1,$$

where $\theta = 4 \cdot N_e \cdot u$ denote the population mutation rate, and u the per nucleotide, per generation molecular mutation rate.

Comparing genomes from two distinct (sub)species, therefore potentially encompassing larger time scales, Mailund et al. used a fully parametrised substitution model as used in parametric phylogenetic reconstruction methods [22]. The mutation process is then a continuous time, discrete-state Markov model with generator U , and the emission probabilities are given by $\exp(U \cdot t_j)$ for each hidden state j . In both models, the emission probabilities only depend on the observed states and are independent of the actual position in the sequence, assuming a homogeneous mutation process along the genome.

1.6. The three-genome case. In 2007, Hobolth et al. introduced the first CoalHMM model [27], by modelling the possible genealogical relationships between three species: “ $(A, B), C$ ”, “ $A, (B, C)$ ” and “ $(A, C), B$ ” (Figure 3B). Considering the two speciation events that separate first the ancestor of A and B from the ancestor of C , and then the ancestor of A from the ancestor of B , the probability that an individual sequence from A coalesces with a sequence from B within the AB ancestral species depends on the ancestral population size and the time between the two speciation events [19]. Backwards in time, if the two corresponding lineages do not coalesce until the most ancient speciation time, any of them can coalesce with a sequence from species C before coalescing with each other. This phenomenon, which results in the marginal genealogy being incongruent with the phylogeny, is termed *incomplete lineage sorting (ILS)*. Using coalescent theory, Hobolth et al. derived relationships between the transition probabilities and used them to infer ancestral effective population sizes as well as the dates of species divergence, the so-called speciation times. In this first model the hidden states differ in tree topology and divergence times. The first hidden state corresponds to the case where the two lineages A and B coalesce within the ancestral population of A and B , leading to a genealogy congruent with the phylogeny. The three other topologies denote cases where the A and B lineages did not coalesce within the AB ancestor, so that the three lineages A , B and C were already present within the ancestral population of the three species. These three states correspond to the cases where A and B , A and C , or B and C coalesce first, respectively (Figure 3B). The model assumes constant ancestral population sizes and the divergence times for each topology are reduced to the averages of the corresponding exponential distributions. The proportion of ILS topologies directly depends on the time separating the speciation events Δ_T and the effective size of the ancestral population θ_{anc} [19]:

$$(8) \quad \Pr(ILS) = \frac{2}{3} \exp\left(-2 \cdot \frac{\theta_{\text{anc}}}{\Delta_T}\right),$$

allowing the estimations of these parameters from the patterns of topology variation. The three-species CoalHMM model was applied to genome sequences of Great Apes: Orangutan [28], Gorilla [60], Bonobo [56], Baboons [58], in order to infer the patterns of ILS and the ancestral effective population sizes in this group of species (reviewed in [44]). It was also applied to species of fungal pathogens where it was used to infer recombination rates [73].

1.7. The multiple-genome cases. With the development of sequencing technologies and the increasing sample size of population genomic datasets, models able to extract the genealogical information contained in multiple genomes are needed. Building CoalHMM models with more than two or three sequences poses, however, a computational challenge because of the underlying combinatorics of marginal genealogies. The number of possible topologies increases hyper-exponentially with the number M of sampled sequences, and there is an infinite number of possible genealogies with a given topology due to the continuous nature of branch lengths (divergence

times). Further approximations are, therefore, required to scale CoalHMM approaches with larger datasets.

1.7.1. *Using conditional sampling distributions.* In a series of articles [54, 70, 62, 69], Song and collaborators developed an approach based on the so-called *conditional sampling distribution* (CSD) introduced by Li and Stephens [40]. This approach stems from the chain rule of conditional probabilities, allowing the expression of the likelihood of a sample of M sequences S_1, \dots, S_M as a product of conditional likelihoods:

$$\begin{aligned} (9) \quad \Pr(S_1, S_2, \dots, S_M | \Theta) &= \Pr(S_1 | S_2, \dots, S_M, \Theta) \cdot \Pr(S_2, \dots, S_M | \Theta) \\ &= \Pr(S_1 | S_2, \dots, S_M, \Theta) \cdot \Pr(S_2 | S_3, \dots, S_M | \Theta) \cdot \Pr(S_3, \dots, S_M | \Theta) \\ &= \Pr(S_M | \Theta) \prod_{k=1}^{M-1} \Pr(S_k | S_{k+1}, \dots, S_M, \Theta), \end{aligned}$$

where Θ denotes the parameter vector. The conditional likelihoods, however, are approximated, so that the resulting likelihood is a product of approximate conditionals (PAC) [40], which depends on the order by which the sequences are treated in the product chain. This is usually accommodated by permutations and averaging [40], or by a composite likelihood approach such as the “leave-one-out” strategy [62]:

$$(10) \quad \Pr(S_1, S_2, \dots, S_M | \Theta) \simeq \prod_{i=1}^M \Pr(S_i | \{S_j\}_{j \neq i}, \Theta).$$

The CSD are computed under an SMC model, given a piecewise constant demographic model, as in the PSMC. The model was further extended to allow more complex demographic scenarios with population structure and migration [69].

1.7.2. *Modelling the most recent coalescence events.* Schiffels and Durbin [61] developed the *multiple sequentially Markov coalescent (MSMC)*, which models only the most recent coalescent event in the sample. The underlying rationale was that the PSMC is lacking resolution in the more recent past, due to the very small number of mutations and coalescences happening in the most recent epochs. Combining multiple samples, therefore, has the potential to compensate for the lack of information in a single pair of genomes. The MSMC approach is elegant as it reduces the combinatorics of the hidden states to one continuous variable (which is discretised, as in the PSMC): the time of coalescence, together with the index of the two genomes in the sample that are coalescing, bringing the number of hidden states to $n = \binom{M}{2} \cdot K$, where K is the number of discrete classes used for the distribution of divergence times. The efficiency of the MSMC approach is, however, paradoxical: by gaining resolution in the present as the sample size increases, the method progressively loses power as the number of modelled sequences becomes larger (see [17] for an illustration). In practice, the authors showed that for a human dataset, the maximum resolution is obtained for eight haploid genomes [61].

1.7.3. *Using a composite likelihood.* In the MSMC2 approach [45, 78], Schiffels and collaborators proposed to approximate the likelihood of a sample of M genomes by independently considering all pairs of genomes. The likelihood of the sample is then approximated by the product of all pairwise likelihoods, each computed under the PSMC model. While the pairwise likelihoods are exact under the SMC, the likelihood of the sample is an example of *composite likelihood* [36]:

$$(11) \quad \Pr(S_1, S_2, \dots, S_M | \Theta) \simeq \prod_{i=1}^{M-1} \prod_{j=i+1}^M \Pr(S_i, S_j | \Theta).$$

The likelihood here is an approximation since the divergence times between pairs of sequences in a genealogy are not independent. The MSMC2 approach is therefore better described as a “multiple pairwise SMC”. It was shown to display good resolution in both the past and present time, efficiently making use of the increasing quantity of signal as the sample size increases.

1.7.4. *Augmenting the PSMC with site frequency spectra.* While approaches like diCal and MSMC2 allow for the efficient modelling of the evolution of multiple genomes, they are intrinsically limited as the computational cost become prohibitive for samples of more than one or two dozen genomes (at least for genomes with a size of the order of that of humans). Terhorst and colleagues introduced a hybrid approach combining the power of the SMC, which makes efficient use of linkage patterns, with that of classical site frequency spectrum (SFS) based approaches [76]. This modelling framework, termed SMC++, considers a “focus” diploid individual that is modelled with a PSMC approach. The observed states are then augmented by taking into account additional genomes to compute an SFS. The emission probabilities are calculated as the probability of observing the local SFS given the genealogy at the focus individual, and the authors proposed an approach to compute such a conditional site frequency spectrum (CSFS). The resulting SMC++ model can accommodate hundreds of individual genomes. Another innovation introduced in this approach is the abandonment of the “skyline” model of piecewise constant effective population size in favour of a spline model. While divergence times are still discretised, the corresponding times for each category are derived from a spline curve whose parameters are estimated. This reduces the number of parameters to estimate and ensures smoother inferred demographies. The SMC++ approach has been applied to human data as well as other species, including *Drosophila* and Zebra finch [76].

2. HETEROGENEITY OF PROCESSES ALONG THE GENOME

In all models that we evoked so far, evolutionary processes have been considered to be homogeneous along sequences. In this section, I review evidence that these assumptions are at odds with our current knowledge of the biology of genomes.

2.1. Variation of the recombination rate. Recombination rates can vary extensively between species [68], between sexes [37] and within genomes. At the molecular scale, multiple levels can be distinguished: recombination rate correlates negatively with chromosome size, a pattern attributed to the mechanism of meiosis and crossing-over interference [32]. Given that the rate of crossing-over events is low, this leads to a higher recombination rate in small chromosomes. Recombination rates vary also within chromosomes: in Primates, it is generally higher at the start and end of the chromosomes (the so-called telomeric regions) [72], while in *Drosophila* the opposite pattern is observed [13, 10]. In many species recombination events have an increased chance to occur in particular regions, called hotspots [55, 52, 74] (but see [77] for a counterexample).

The variation of recombination rate has two types of consequences on the patterns of sequence diversity. Because the molecular mechanisms of recombination are tightly linked to DNA repair, recombination itself can be mutagenic and locally increase sequence variability [38, 4]. Furthermore, in many species, the repair mechanisms involve gene conversion between homologous sequences, as one chromosome is used as a template to repair the other one. However, this mechanism is biased in many species: in the case of heterozygous positions, the “C” or “G” nucleotides are preferred over “A” and “T” nucleotides, potentially resulting in large scale variations of GC content [16] mirroring the variations in recombination rate. The recombination rate also has indirect effects on genetic diversity: because it breaks down genetic linkage, recombination counteracts the reduction of diversity at sites linked to loci under selection, both negative (background selection [11]) and positive (genetic hitch-hiking [9]). By modulating the local effective population size, variation of recombination rate along the genome has a strong impact on the underlying genealogy.

2.2. Variation of the mutation rate. Finally, the rate at which mutations occur can vary extensively along the genome [7]. Mutations can occur via direct modification of the DNA or indirectly, via errors in the replication or repair mechanisms. Particular sequence motifs, such as CpG dinucleotides are known to undergo comparatively higher mutation rates, via the methylation of the cytosine, which is then deaminated into a thymine, leading to a TpG dinucleotide. In addition to the potentially mutagenic effect of recombination, which also plays a role in the repair of DNA damage, the replication machinery itself is error-prone. This error rate is position dependent: it increases with the replication time, being lower close to the origins of replication [67, 3, 79]. Under a neutral scenario, the mutation process is independent of the coalescent process [30], and, therefore, has no impact on the underlying genealogies. Yet, for inference models, mutation rate variation acts as a confounding factor, as a high sequence divergence can be either explained by an ancient coalescence time or a high mutation rate. In CoalHMM models, the mutation rate will have an impact on the emission probabilities, that is, the probability of observing the observed sequence diversity given a genealogy.

3. EXISTING APPROACHES TO ACCOUNT FOR SPATIAL HETEROGENEITY

In this section, I review the approaches that have been developed to cope with the heterogeneity of evolutionary processes acting along the genome.

3.1. Inferring sequential heterogeneity alone. A large body of work is built on the idea that, if a parameter affects certain patterns of genetic diversity, it should be possible to use these patterns to recover the underlying variation of the parameter. The most studied case in this respect is the recombination rate, via its impact on linkage disequilibrium. Given an a priori known demographic scenario, it is possible to compute the likelihood of the data for any given recombination rate, and use it to estimate the most likely recombination rate value. Due to the complexity of the underlying model, however, approximations are required to apply these methods to large genomic datasets. McVean, Awadalla and Fearnhead [48] introduced the use of a composite likelihood, approximating the full likelihood by the product of the likelihoods of all pairs of positions within a minimum distance of each other. This approach is the basis of several popular methods for recombination rate inference such as LDhat [5] and LDhelmet [10]. Further developments of these models allowed for the incorporation of variable population sizes [33, 64]. The underlying demography, however, has to be estimated independently from the data. Li and Stephens [40], on the other hand, used the conditional sampling distribution and the product of approximate conditionals (PAC) to approximate the likelihood. An application of this method also includes the reconstruction of haplotypes from genotypic data, a problem known as *phasing* [71].

3.2. Inference using piecewise-homogeneous processes. The most simple approach to infer heterogeneous processes along the genome while jointly accounting for demography is to use a window-based approach, consisting of dividing the genome into segments of fixed sizes and estimating model parameters independently in each resulting window. This strategy was used by Stukenbrock et al. [73] to use the patterns of ILS and a CoalHMM model to estimate the recombination rate in 100 kb windows along the genome of the fungal pathogen *Zymoseptoria tritici*. In most cases, however, SMC models require long genome sequences to be able to confidently estimate parameters, and cannot be run in windows of small sizes, in particular for models at the population level. Furthermore, window-based approaches raise the issue of the window size and boundaries to use.

3.3. Using sequentially heterogeneous simulation procedures. While the computation of the likelihood of the data under a sequentially heterogeneous process is notoriously difficult, simulating under the corresponding model can be comparatively easy. Software like the Markovian coalescent simulator (MaCS) [12], the sequential coalescent with recombination model (SCRM) [66], fastsimcoal [21] and MSprime [34] allow the simulation of population genomic data sets under models with variable recombination rate. Owing to their high computational efficiency, they can be used within an approximate Bayesian computation (ABC) framework in order to estimate demographic parameters under realistic recombination models [80]. This

possibility, however, has to date been underexploited, as demographic inference is so far conducted with data simulated under a homogeneous recombination landscape (see for instance [41]). While no ABC method has been developed with the goal to infer the variation of population genomic parameters along the genome, Gao et al. [24] introduced a machine learning approach to infer recombination rates. The underlying simulations, however, are conducted under a model with constant recombination rate.

3.4. A posteriori inference of heterogeneous processes. The HMM methodology allows, via the forward algorithm, to compute the likelihood of the data given a specified demographic model by efficiently integrating over the unknown underlying ARG. The HMM toolbox further allows for the computation of the a posteriori probability of each marginal genealogy for each position [17]:

$$(12) \quad \Pr(\mathcal{H}_i = H_j \mid x_1, \dots, x_L) = \frac{\Pr(x_1, \dots, x_L, \mathcal{H}_i = H_j)}{\Pr(x_1, \dots, x_L)}.$$

The denominator of the ratio is the likelihood of the data, \mathcal{L} . In order to compute the numerator, we need to introduce the so-called *backward algorithm* [15]:

$$(13) \quad B_{i,j} = \Pr(x_{i+1}, \dots, x_L \mid \mathcal{H}_i = H_j) = \begin{cases} 1 & \text{if } i = L \\ \sum_k e_{i+1,k}(x_{i+1}) \cdot q_{i+1,j,k} \cdot B_{i+1,k} & \text{if } i < L, \end{cases}$$

The posterior probability of hidden state H_j can therefore be computed as

$$(14) \quad \Pr(\mathcal{H}_i = H_j \mid x_1, \dots, x_L) = \frac{F_{i,j} \cdot B_{i,j}}{\mathcal{L}}.$$

This formula allows for the reconstruction of the most probable marginal genealogy at each position i by taking the maximum posterior probability

$$(15) \quad \hat{\mathcal{H}}_i = \arg \max_j (\Pr(\mathcal{H}_i = H_j \mid x_1, \dots, x_L)),$$

a procedure called *posterior decoding*. The posterior decoding is performed after fitting the model parameters by maximizing the likelihood. It is therefore an example of *empirical Bayesian* inference [46].

Posterior probabilities of marginal genealogies can also be used to obtain posterior estimates of biological quantities of interest, accounting for the uncertainty on the underlying genealogy. The posterior mean estimate $\hat{\lambda}_i$ at position i of a property $\Lambda(H_j)$ can be obtained by

$$(16) \quad \hat{\lambda}_i = \sum_j \Pr(\mathcal{H}_i = H_j \mid x_i, \dots, x_L) \cdot \Lambda(H_j).$$

If Λ is the coalescence time between two sequences, this formula can be used to get posterior estimates of sequence divergence along the genome [53]. More complex examples of functions include, for instance, whether \mathcal{H}_i is distinct from \mathcal{H}_{i-1} , or, in other words, whether a recombination event occurred between positions i and $i-1$. This allows for the reconstruction of a recombination map, integrating over the ARG. Such approach was notably used by Munch et al [51] to reconstruct the recombination map of the human-chimpanzee ancestor. Posterior estimates are rather robust to the specified

input model and can therefore offer a powerful approach to infer aspects of the process that are not directly accounted for by the model. However, because some model properties are intrinsically confounded, such as local divergence and mutation rate, ignoring spatial heterogeneity might result in biased inference [8].

4. THE INTEGRATIVE SEQUENTIALLY MARKOV COALESCENT

In order to account for heterogeneous processes along the genome, we recently developed the integrative sequentially Markov coalescent (iSMC) [8], an extension of the SMC. In this framework, parameters of the original SMC vary along the genome in a Markovian manner, allowing for the modelling of genome heterogeneity in addition to demographic processes. I illustrate this approach with results from a recent application of this framework to infer recombination landscapes and further discuss possible extensions.

4.1. The Markov-modulated sequentially Markov coalescent. Whilst the framework can be applied to cases where more than one parameter varies along the genome, for simplicity, we here consider the case where one parameter only varies, which we label \mathcal{R} , \mathcal{R}_i denoting the values of \mathcal{R} at position i in the sequences. We assume that \mathcal{R} follows an a priori known discrete distribution with n^R categories, each with mean value R_k , with $1 \leq k \leq n^R$. In the iSMC framework, the transition and/or emission probabilities are functions of \mathcal{R} and are, therefore, noted as $e_{i,k}^{\text{SMC}}(x, R)$ and $q_{i,j,k}^{\text{SMC}}(R)$, respectively. The key assumption is then to consider that the variation of \mathcal{R} along the genome can be modelled as a Markov model, that is, there is a matrix of probabilities q^R defined as

$$(17) \quad q_{i,j,k}^R = \Pr(\mathcal{R}_i = R_k \mid \mathcal{R}_{i-1} = R_j).$$

The forward recursion of the CoalHMM can then be written as

$$(18) \quad F_{i,j,k}^{\text{SMC}} = \Pr(x_1, \dots, x_i, H_j, R_k) = \begin{cases} f_j \cdot f_k^R & \text{if } i = 0 \\ e_{i,j}^{\text{SMC}}(x_i, R_k) \cdot \sum_u \sum_v q_{i,u,j}^{\text{SMC}}(R_k) \cdot q_{i,v,k}^R \cdot F_{i-1,u,v}^{\text{SMC}} & \text{if } i > 0, \end{cases}$$

where f_k^R denotes the a priori probability $\Pr(\mathcal{R} = R_k)$. Because the SMC now depends on a parameter that itself follows a Markov process, the resulting process can be described as a Markov-modulated Markov chain (MMMC). As an MMMC is itself a Markov process [23], we can rewrite the forward recursion as:

$$(19) \quad F_{i,k}^{\text{iSMC}} = \Pr(x_1, \dots, x_i, H_k^{\text{iSMC}}) = \begin{cases} f_k^{\text{iSMC}} & \text{if } i = 0 \\ e_{i,k}^{\text{iSMC}}(x_i) \cdot \sum_j q_{i,j,k}^{\text{iSMC}} \cdot F_{i-1,j}^{\text{iSMC}} & \text{if } i > 0. \end{cases}$$

In the iSMC hidden Markov model, the hidden states H^{iSMC} consist of all possible pairs of genealogies and \mathcal{R} : (R_a, H_b) , with $1 \leq a \leq n^R$ and $1 \leq b \leq n$. The emission probabilities $e_{i,j}^{\text{iSMC}}(x)$ now depend on the pair $(R, H)_j$, and the initial probabilities of the hidden states are $f^{\text{iSMC}} = f^R \otimes f$. Similarly, the transition probabilities of the Markov-modulated SMC (MMSMC) can

be written as a function of the transition probabilities of the two Markov chains:

$$(20) \quad q_i^{\text{iSMC}} = \begin{pmatrix} q_{i,1,1}^R \cdot q_i^{\text{SMC}}(R_1) & \cdots & q_{i,1,n^R}^R \cdot q_i^{\text{SMC}}(R_1) \\ \vdots & \ddots & \vdots \\ q_{i,n^R,1}^R \cdot q_i^{\text{SMC}}(R_{(n^R)}) & \cdots & q_{i,n^R,n^R}^R \cdot q_i^{\text{SMC}}(R_{(n^R)}) \end{pmatrix}.$$

(As we consider the process modelling the variation of \mathcal{R} to be itself homogeneous along the genome, we have $\forall i_1, i_2, q_{i_1,j,k}^{\text{iSMC}} = q_{i_2,j,k}^{\text{iSMC}} = q_{j,k}^{\text{iSMC}}$.) The iSMC model can therefore be analysed with standard HMM methodology, just like the homogeneous SMC. The number of hidden states, however, is now $n^R \cdot n$, meaning that the complexity of the likelihood calculation becomes $\mathcal{O}(L \cdot (n \cdot n^R)^2)$.

The iSMC model adds relatively few extra parameters to the SMC: the transition probabilities q^R , which can be reduced to one parameter (see below), and parameters of the a priori distribution of \mathcal{R} . While parameters of the distribution of \mathcal{R} are generally not of direct biological interest, the posterior decoding of the HMM allows for the inference of the underlying landscape of the heterogeneous parameter. Distinct decoding procedures can be performed in the case of Markov-modulated HMMs:

- (1) A full decoding, where the most likely pair (R, H) at each position is reconstructed:

$$(21) \quad (\widehat{\mathcal{R}}, \widehat{\mathcal{H}})_i = \arg \max_{j,k} (\Pr(\mathcal{H}_i = H_j, \mathcal{R}_i = R_k \mid x_i, \dots, x_L)),$$

- (2) A partial decoding of genealogies, where the most likely genealogy is inferred, summing over all heterogeneous parameters:

$$(22) \quad \hat{\mathcal{H}}_i = \arg \max_j \left(\sum_k \Pr(\mathcal{H}_i = H_j, \mathcal{R}_i = R_k \mid x_i, \dots, x_L) \right),$$

- (3) A posterior mean estimation of the heterogeneous variable. Setting $\Lambda(H_j, R_j) = R_j$ and applying equation 16, we get:

$$(23) \quad \hat{\mathcal{R}}_i = \sum_j \sum_k \Pr(\mathcal{H}_i = H_j, \mathcal{R}_i = R_k \mid x_i, \dots, x_L) \cdot R_k \\ = \sum_k R_k \cdot \sum_j \Pr(\mathcal{H}_i = H_j, \mathcal{R}_i = R_k \mid x_i, \dots, x_L).$$

The partial decoding of genealogies enables the reconstruction of the ARG while accounting for the heterogeneity of the SMC along the genome. The posterior estimates of the heterogeneous variable allows the reconstruction of the variation along the genome while accounting for the genealogy and its uncertainty. In the next section, we apply this framework to model the variation of the recombination rate along the genome.

4.2. A case study: inference of recombination rate variation. Recombination is the best documented heterogeneous process along the genome. It can be measured experimentally or indirectly using genomic approaches (reviewed in [5]). In the context of the sequential coalescent and the SMC

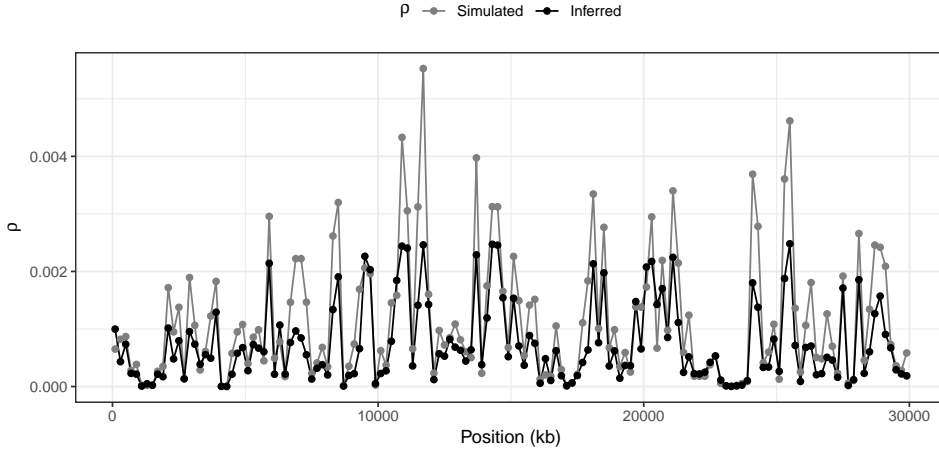


FIGURE 5. Posterior estimates of recombination rates from a single diploid genome using iSMC. A 30 Mb region was simulated using the SCRIM program [66] and a variable recombination rate, and then inferred with iSMC, as described in [8]. Recombination rates were averaged in windows of 200 kb.

approximation, the local recombination rate affects the probability of transition from one genealogy to another, which increases with higher recombination rates. To model variable recombination rates in iSMC, we considered that the local population recombination rate $\rho = 4 \cdot N_e \cdot r$, where r is the molecular recombination rate in cM / bp per generation, is the product of a genome average ρ_G and a local modifier r^ρ . This modifier follows a prior discrete distribution of mean 1 and with n^ρ categories, for instance a discretised Gamma distribution with shape parameter α . We further considered a simple model for the transition probabilities between the r^ρ classes, assuming equal probabilities of change, γ . The transition probability matrix q^ρ takes the form:

$$(24) \quad q^\rho = \begin{pmatrix} 1 - \gamma & \gamma/(n^\rho - 1) & \cdots & \gamma/(n^\rho - 1) \\ \gamma/(n^\rho - 1) & 1 - \gamma & \ddots & \vdots \\ \vdots & \ddots & \ddots & \gamma/(n^\rho - 1) \\ \gamma/(n^\rho - 1) & \cdots & \gamma/(n^\rho - 1) & 1 - \gamma \end{pmatrix}.$$

Using the forward equation 19, we can compute the likelihood of the parameters of the iSMC model. Using optimisation procedures, estimates of the α and γ parameters together with the average ρ_G and the demography parameters can be obtained by maximizing the likelihood function. The likelihood calculation can also be used to perform model comparisons and test for the heterogeneity of the coalescent process along the genome, for instance using Akaike's information criterion (AIC).

A posterior decoding approach (equation 23) can then be used to obtain estimates of site-specific recombination rates. Simulations under controlled

recombination landscape and demography can be used to assess the accuracy of the iSMC inference [8]. Figure 5 shows that iSMC recovers the underlying recombination landscape with good accuracy, despite generally underestimating high recombination rates. A possible explanation for this is the discretisation procedure, as the posterior mean estimate is bounded by the class with the highest mean recombination value. Allowing for more recombination classes allows for a wider range of values and can potentially reduce this bias, at the cost of increasing the running time and memory usage. Because it can recover the recombination landscape from a single diploid only, the iSMC model was used to generate recombination maps from extinct hominids from their ancient genome sequences [8].

4.3. Extension of iSMC: multiple genomes and multiple heterogeneous parameters. The Markov-modulated Markov model framework underlying the iSMC approach can be applied to other SMC models, such as the MSMC [61]. Hidden states of the resulting CoalHMM are combinations of TMRCA, pairs of genome indices undergoing the most recent coalescent event, and classes of heterogeneous parameters such as the recombination rate. Extension to multiple genomes can also be achieved using a composite likelihood approach, as implemented in MSMC2 (see 1.7.3). The likelihood of the dataset is then approximated by the product of the likelihoods of each pair of genomes, which are modelled separately with their own process. In the case of the iSMC approach, this implies considering that the heterogeneous parameters vary independently along each pair of genomes; for a model with variable recombination rate, this is equivalent to estimating a distinct recombination map for each pair of genomes. This assumption is clearly incorrect for the vast majority of positions within genomes from the same population. Extensions enforcing a common map while allowing the coalescent processes to be independent will, therefore, be instrumental in efficiently scaling the iSMC approach to larger sample sizes.

The iSMC framework further allows the joint modelling of the variation of multiple parameters along the genome, such as the mutation and recombination rates. In such approach, the hidden states are a combination of TMRCA and classes for each discretised parameter. The addition of any additional heterogeneous parameter multiplies the complexity of the likelihood calculation by n^{ϕ^2} , where n^{ϕ} is the number of discrete classes considered for the parameter distribution. Besides the increased complexity, identifiability issues may also arise, since local patterns of diversity may be equally explained by variation of demography, recombination rate or mutation rate.

However, when these parameters vary at a scale larger than the variation of the TMRCA along the genome and when very large genome sequences are analyzed, increasingly complex models may be successfully fitted.

5. CONCLUSIONS

The availability of complete genome data opened the floodgates for the detailed inference of the demographic history of species. A new generation of coalescent-based models permits the extraction of demographic signal from the patterns of genetic linkage along sequences. Such models, however,

largely ignore fundamental aspects of genome biology, that is, that processes such as recombination and mutation are highly heterogeneous along genomes. Extending these approaches to account for such heterogeneity not only potentially improves demographic inference, but also allows to reconstruct the underlying genomic landscape.

Acknowledgement. I would like to thank Gustavo V. Barroso for critical reading of this manuscript and for providing the simulation data plotted in Figure 5. I am deeply indebted to Ellen Baake, as well as Jeffrey P. Spence and an anonymous reviewer for their careful reading of the manuscript, for finding several mistakes and typos, and for their suggestions on how to improve its clarity.

REFERENCES

- [1] 1000 Genomes Project Consortium (and 8 coauthors), A map of human genome variation from population-scale sequencing, *Nature* **467** (2010), 1061–1073.
- [2] A.M. Adams and R.R. Hudson, Maximum-likelihood estimation of demographic parameters using the frequency spectrum of unlinked single-nucleotide polymorphisms, *Genetics* **168** (2004), 1699–1712.
- [3] N. Agier and G. Fischer, The mutational profile of the yeast genome is shaped by replication, *Mol. Biol. Evol.* **29** (2012), 905–913.
- [4] I. Alves, A.A. Houle, J.G. Hussin, and P. Awadalla, The impact of recombination on human mutation load and disease, *Philos. Trans. R. Soc. Lond. B, Biol. Sci.* **372** (2017), 20160465.
- [5] A. Auton and G. McVean, Estimating recombination rates from genetic variation in humans, *Methods Mol. Biol.* **856** (2012), 217–237.
- [6] E. Baake and M. Baake, Ancestral lines under recombination, *this volume*.
- [7] C.F. Baer, M.M. Miyamoto, and D.R. Denver, Mutation rate variation in multicellular eukaryotes: causes and consequences, *Nature Reviews Genetics* **8** (2007), 619–631.
- [8] G.V. Barroso, N. Puzovic, and J. Dutheil, Inference of recombination maps from a single pair of genomes and its application to archaic samples, *PLoS Genet.* **15** (2019), e1008449.
- [9] N.H. Barton, Genetic hitchhiking, *Philos. Trans. R. Soc. Lond. B, Biol. Sci.* **355** (2000), 1553–1562.
- [10] A.H. Chan, P.A. Jenkins, and Y.S. Song, Genome-wide fine-scale recombination rate variation in *Drosophila melanogaster*, *PLoS Genet.* **8** (2012), e1003090.
- [11] B. Charlesworth, M.T. Morgan, and D. Charlesworth. The effect of deleterious mutations on neutral molecular variation, *Genetics* **134** (1993), 1289–1303.
- [12] G.K. Chen, P. Marjoram, and J.D. Wall, Fast and flexible simulation of DNA sequence data, *Genome Res.* **19** (2009), 136–142.
- [13] J.M. Comeron, R. Ratnappan, and S. Bailin, The many landscapes of recombination in *Drosophila melanogaster*, *PLoS Genet.* **8** (2012), e1002905.
- [14] A.J. Drummond, A. Rambaut, B. Shapiro, and O.G. Pybus, Bayesian coalescent inference of past population dynamics from molecular sequences, *Mol. Biol. Evol.* **22** (2005), 1185–1192.
- [15] R. Durbin, S.R. Eddy, A. Krogh, and G. Mitchison, *Biological Sequence Analysis: Probabilistic Models of Proteins and Nucleic Acids*, Cambridge University Press, Cambridge, 1998.
- [16] L. Duret and N. Galtier, Biased gene conversion and the evolution of mammalian genomic landscapes, *Annu. Rev. Genomics Hum. Genet.* **10** (2009), 285–311.
- [17] J.Y. Dutheil, Hidden Markov models in population genomics, *Methods Mol. Biol.* **1552** (2017), 149–164.

- [18] J.Y. Dutheil, G. Ganapathy, A. Hobolth, T. Mailund, M.K. Uyenoyama, and M.H. Schierup, Ancestral population genomics: the coalescent hidden Markov model approach, *Genetics* **183** (2009), 259–274.
- [19] J.Y. Dutheil and A. Hobolth, Ancestral population genomics, *Methods Mol. Biol.* **856** (2012), 293–313.
- [20] S.N. Ethier and R.C. Griffiths, On the two-locus sampling distribution, *J. Math. Biol.* **29** (1990), 131–159.
- [21] L. Excoffier and M. Foll, fastsimcoal: a continuous-time coalescent simulator of genomic diversity under arbitrarily complex evolutionary scenarios, *Bioinformatics* **27** (2011), 1332–1334.
- [22] J. Felsenstein, *Inferring Phylogenies*, 2nd ed., Sinauer, Sunderland, MA, 2003.
- [23] N. Galtier and A. Jean-Marie, Markov-modulated Markov chains and the covarian process of molecular evolution, *J. Comput. Biol.* **11** (2004), 727–733.
- [24] F. Gao, C. Ming, W. Hu, and H. Li, New software for the fast estimation of population recombination rates (FastEPRR) in the genomic era, *G3* **6** (2016), 1563–1571.
- [25] R.C. Griffiths and P. Marjoram, Ancestral inference from samples of DNA sequences with recombination, *J. Comput. Biol.* **3** (1996), 479–502.
- [26] K. Harris, S. Sheehan, J.A. Kamm, and Y.S. Song, Decoding coalescent hidden Markov models in linear time. In: *Research in Computational Molecular Biology. RECOMB2014*, R. Sharan (ed.), Springer, Cham, 2014, pp. 100–114.
- [27] A. Hobolth, O.F. Christensen, T. Mailund, and M.H. Schierup, Genomic relationships and speciation times of human, chimpanzee, and gorilla inferred from a coalescent hidden Markov model, *PLoS Genet.* **3** (2007), e7.
- [28] A. Hobolth, J.Y. Dutheil, J. Hawks, M.H. Schierup, and T. Mailund, Incomplete lineage sorting patterns among human, chimpanzee, and orangutan suggest recent orangutan speciation and widespread selection, *Genome Res.* **21** (2011), 349–356.
- [29] A. Hobolth and J.L. Jensen, Markovian approximation to the finite loci coalescent with recombination along multiple sequences, *Theor. Popul. Biol.* **98** (2014), 48–58.
- [30] R.R. Hudson, Properties of a neutral allele model with intragenic recombination, *Theor. Popul. Biol.* **23** (1983), 183–201.
- [31] R.R. Hudson, Generating samples under a Wright–Fisher neutral model of genetic variation, *Bioinformatics* **18** (2002), 337–338.
- [32] D.B. Kaback, Chromosome-size dependent control of meiotic recombination in humans, *Nat. Genet.* **13** (1996), 20–21.
- [33] J.A. Kamm, J.P. Spence, J. Chan, and Y.S. Song, Two-locus likelihoods under variable population size and fine-scale recombination rate estimation, *Genetics* **203** (2016), 1381–1399.
- [34] J. Kelleher, A.M. Etheridge, and G. McVean, Efficient coalescent simulation and genealogical analysis for large sample sizes, *PLoS Comput. Biol.* **12** (2016), e1004842.
- [35] J.F.C. Kingman, The coalescent, *Stochastic Processes Appl.* **13** (1982), 235–248.
- [36] F. Larribe and P. Fearnhead, On composite likelihoods in statistical genetics, *Statistica Sinica* **21** (2011), 43–69.
- [37] T. Lenormand and J. Dutheil, Recombination difference between sexes: a role for haploid selection, *PLoS Biol.* **3** (2005), e63.
- [38] M.J. Lercher and L.D. Hurst, Human SNP variability and mutation rate are higher in regions of high recombination, *Trends Genet.* **18** (2002), 337–340.
- [39] H. Li and R. Durbin, Inference of human population history from individual whole-genome sequences, *Nature* **475** (2011), 493–496.
- [40] N. Li and M. Stephens, Modeling linkage disequilibrium and identifying recombination hotspots using single-nucleotide polymorphism data, *Genetics* **165** (2003), 2213–2233.

- [41] S. Li and M. Jakobsson, Estimating demographic parameters from large-scale population genomic data using Approximate Bayesian Computation, *BMC Genet.* **13** (2012), 22–37.
- [42] T. Mailund, J.Y. Dutheil, A. Hobolth, G. Lunter, and M.H. Schierup, Estimating divergence time and ancestral effective population size of Bornean and Sumatran orangutan subspecies using a coalescent hidden Markov model, *PLoS Genet.* **7** (2011), e1001319.
- [43] T. Mailund, A.E. Halager, M. Westergaard, J.Y. Dutheil, K. Munch, L.N. Andersen, G. Lunter, K. Prüfer, A. Scally, A. Hobolth, and M.H. Schierup, A new isolation with migration model along complete genomes infers very different divergence processes among closely related great ape species, *PLoS Genet.* **8** (2012), e1003125.
- [44] T. Mailund, K. Munch, and M.H. Schierup, Lineage sorting in apes, *Annu. Rev. Genet.* **48** (2014), 519–535.
- [45] A.-S. Malaspinas (and 74 coauthors), A genomic history of Aboriginal Australia, *Nature* **538** (2016), 207–214.
- [46] J.S. Maritz and T. Lwin, *Empirical Bayes Methods*, Routledge, London, 2018.
- [47] P. Marjoram and J.D. Wall, Fast “coalescent” simulation, *BMC Genet.* **7** (2006), 16.
- [48] G. McVean, P. Awadalla, and P. Fearnhead, A coalescent-based method for detecting and estimating recombination from gene sequences, *Genetics* **160** (2002), 1231–1241.
- [49] G.A.T. McVean and N.J. Cardin, Approximating the coalescent with recombination, *Philos. Trans. R. Soc. Lond. B, Biol. Sci.* **360** (2005), 1387–1393.
- [50] P.A.P. Moran, Random processes in genetics, *Math. Proc. Camb. Phil. Soc.*, **54** (1958), 60–71.
- [51] K. Munch, T. Mailund, J.Y. Dutheil, and M.H. Schierup, A fine-scale recombination map of the human-chimpanzee ancestor reveals faster change in humans than in chimpanzees and a strong impact of GC-biased gene conversion, *Genome Res.* **24** (2014), 467–474.
- [52] S. Myers, L. Bottolo, C. Freeman, G. McVean, and P. Donnelly, A fine-scale map of recombination rates and hotspots across the human genome, *Science* **310** (2005), 321–324.
- [53] P.F. Palamara, J. Terhorst, Y.S. Song, and A.L. Price, High-throughput inference of pairwise coalescence times identifies signals of selection and enriched disease heritability, *Nat. Genet.* **50** (2018), 1311–1317.
- [54] J.S. Paul, M. Steinrücken, and Y.S. Song, An accurate sequentially Markov conditional sampling distribution for the coalescent with recombination, *Genetics* **187** (2011), 1115–1128.
- [55] T.D. Petes, Meiotic recombination hot spots and cold spots, *Nature Reviews Genetics* **2** (2001), 360–369.
- [56] K. Prüfer (and 40 coauthors), The bonobo genome compared with the chimpanzee and human genomes, *Nature* **486** (2012), 527–531.
- [57] M.D. Rasmussen, M.J. Hubisz, I. Gronau, and A. Siepel, Genome-wide inference of ancestral recombination graphs, *PLoS Genet.* **10** (2014), e1004342.
- [58] J. Rogers (and 41 coauthors), The comparative genomics and complex population history of *Papio* baboons, *Sci. Adv.* **5** (2019), eaau6947.
- [59] A. Sand, M. Kristiansen, C.N.S. Pedersen, and T. Mailund, zipHMMLib: a highly optimised HMM library exploiting repetitions in the input to speed up the forward algorithm, *BMC Bioinformatics* **14** (2013), 339–348.
- [60] A. Scally (and 70 coauthors), Insights into hominid evolution from the gorilla genome sequence, *Nature* **483** (2012), 169–175.
- [61] S. Schiffels and R. Durbin, Inferring human population size and separation history from multiple genome sequences, *Nat. Genet.* **46** (2014), 919–925.

- [62] S. Sheehan, K. Harris, and Y.S. Song, Estimating variable effective population sizes from multiple genomes: a sequentially markov conditional sampling distribution approach, *Genetics* **194** (2013), 647–662.
- [63] K.L. Simonsen and G.A. Churchill, A Markov chain model of coalescence with recombination, *Theor. Popul. Biol.* **52** (1997), 43–59.
- [64] J.P. Spence and Y.S. Song, Inference and analysis of population-specific fine-scale recombination maps across 26 diverse human populations, *Sci. Adv.* **5** (2019), eaaw9206.
- [65] J.P. Spence, M. Steinrücken, J. Terhorst, and Y.S. Song, Inference of population history using coalescent HMMs: review and outlook, *Curr. Opin. Genet. Dev.* **53** (2018), 70–76.
- [66] P.R. Staab, S. Zhu, D. Metzler, and G. Lunter, scrm: efficiently simulating long sequences using the approximated coalescent with recombination, *Bioinformatics* **31** (2015), 1680–1682.
- [67] J.A. Stamatoyannopoulos, I. Adzhubei, R.E. Thurman, G.V. Kryukov, S.M. Mirkin, and S.R. Sunyaev, Human mutation rate associated with DNA replication timing, *Nat. Genet.* **41** (2009), 393–395.
- [68] J. Stapley, P.G.D. Feulner, S.E. Johnston, A.W. Santure, and C.M. Smadja, Variation in recombination frequency and distribution across eukaryotes: patterns and processes, *Philos. Trans. R. Soc. Lond. B, Biol. Sci.* **372** (2017), 20160455.
- [69] M. Steinrücken, J. Kamm, J.P. Spence, and Y.S. Song, Inference of complex population histories using whole-genome sequences from multiple populations, *Proc. Natl. Acad. Sci. U.S.A.* **116** (2019), 17115–17120.
- [70] M. Steinrücken, J.S. Paul, and Y.S. Song, A sequentially Markov conditional sampling distribution for structured populations with migration and recombination, *Theor. Popul. Biol.* **87** (2013), 51–61.
- [71] M. Stephens and P. Scheet, Accounting for decay of linkage disequilibrium in haplotype inference and missing-data imputation, *Am. J. Hum. Genet.* **76** (2005), 449–462.
- [72] L.S. Stevison (and 9 coauthors) Great Ape Genome Project, The time scale of recombination rate evolution in great apes, *Mol. Biol. Evol.* **33** (2016), 928–945.
- [73] E.H. Stukenbrock, T. Bataillon, J.Y. Dutheil, T.T. Hansen, R. Li, M. Zala, B.A. McDonald, J. Wang, and M.H. Schierup, The making of a new pathogen: insights from comparative population genomics of the domesticated wheat pathogen *Mycosphaerella graminicola* and its wild sister species, *Genome Res.* **21** (2011), 2157–2166.
- [74] E.H. Stukenbrock and J.Y. Dutheil, Fine-scale recombination maps of fungal plant pathogens reveal dynamic recombination landscapes and intragenic hotspots, *Genetics* **208** (2018), 1209–1229.
- [75] M.P.H. Stumpf and G.A.T. McVean, Estimating recombination rates from population-genetic data, *Nat. Rev. Genet.* **4** (2003), 959–968.
- [76] J. Terhorst, J.A. Kamm, and Y.S. Song, Robust and scalable inference of population history from hundreds of unphased whole genomes, *Nat. Genet.* **49** (2017), 303–309.
- [77] A. Wallberg, S. Glémin, and M.T. Webster, Extreme recombination frequencies shape genome variation and evolution in the honeybee, *Apis mellifera*, *PLoS Genet.* **11** (2015), e1005189.
- [78] K. Wang, I. Mathieson, J. O’Connell, and S. Schiffels, Tracking human population structure through time from whole genome sequences, *PLoS Genetics* **16** (2020), 1–24.
- [79] C.C. Weber, C.J. Pink, and L.D. Hurst, Late-replicating domains have higher divergence and diversity in *Drosophila melanogaster*, *Mol. Biol. Evol.* **29** (2012), 873–882.
- [80] D. Wegmann, C. Leuenberger, S. Neuenschwander, and L. Excoffier, ABCtoolbox: a versatile toolkit for approximate Bayesian computations, *BMC Bioinformatics* **11** (2010), 116–123.
- [81] P.R. Wilton, S. Carmi, and A. Hobolth, The SMC’ is a highly accurate approximation to the ancestral recombination graph, *Genetics* **200** (2015), 343–355.

- [82] C. Wiuf and J. Hein, Recombination as a point process along sequences, *Theor. Popul. Biol.* **55** (1999), 248–259.

Email address, J. Y. Dutheil: dutheil@evolbio.mpg.de

RG MOLECULAR SYSTEMS EVOLUTION, MAX PLANCK INSTITUTE FOR EVOLUTIONARY BIOLOGY, AUGUST-THIENEMANN-STR. 2, 24306 PLÖN, GERMANY